JOURNAL OF MATERIALS RESEARCH AND TECHNOLOGY 2022;16:1305–1323

Available online at www.sciencedirect.com

jmr&t Journal of Materials Research and Technology

journal homepage: www.elsevier.com/locate/jmrt

Original Article

Electrochemical action of *Citrus reticulata* and *Pelargonium* oil concentrates on 1018 carbon steel corrosion in anionic solution

Roland Tolulope Loto[*], *Temitayo Ikuerowo*, *Sophia Ifezue*

Department of Mechanical Engineering, Covenant University, Ota, Ogun State, Nigeria

ARTICLE INFO

Article history:
Received 1 November 2021
Accepted 14 December 2021
Available online 22 December 2021

Keywords:
Corrosion
Inhibitor
Oil concentrate
Carbon steel

ABSTRACT

Corrosion inhibition of *Pelargonium* (Pe) and *Citrus reticulata* (Cr) oil concentrates and their admixture (PeCr) on 1018 carbon steel (18CS) was studied in 0.5M H_2SO_4 and HCl media with electrochemical polarization technique, potential-time evaluation (OCP), coupon computation, optical image assessment, ATF-FTIR spectroscopy and X-ray diffractometry. Polarization data showed Pe performed effectively only at the highest concentrations in H_2SO_4 (3% and 3.5%) with optimal inhibition performance of 91.56% while in HCl effective corrosion inhibition occurred at all concentrations considered with optimal value of 87.32% at 2.5% concentration. Cr concentrate performed adequately at all concentrations in H_2SO_4 and HCl solutions with utmost values of 78.12% and 91.87%. PeCr performed more efficiently at all concentrations in HCl with utmost value of 95.46%. PeCr utmost inhibition performance in H_2SO_4 was below 70%. Coupon measurement showed the concentrate performances in HCl are independent of time/concentration, and generally attained stability from 72 to 96 h of exposure. This contrast their performance in H_2SO_4 which is significantly dependent on time/concentration. OCP plots shows the presence of Pe in H_2SO_4 and HCl, Cr in H_2SO_4 and PeCr in H_2SO_4 heightens the thermodynamic tendency of 18CS to corrode in view of its optimal inhibition outputs compared to Cr and PeCr in HCl whose plots decreased the thermodynamic tendency. ATF-FTIR data depict significant decrease in transmittance of reactive groups for Cr in H_2SO_4 and HCl media at all wavenumbers due to adsorption. Transmittance of Pe and PeCr concentrates reactive groups increased after corrosion signifying the nature of their inhibition mechanism. Optical representations of protected and non-inhibited 10CS surfaces substantially differed from each other. X-ray diffractometry identified corrosive precipitates on the steel without concentrate addition. In the presence of the concentrates, in the presence of the concentrates the phases compounds identified on the inhibited steel were non-corrosive.

* Corresponding author.
E-mail address: tolu.loto@gmail.com (R.T. Loto).

https://doi.org/10.1016/j.jmrt.2021.12.067

1. Introduction

The extensive application of carbon steels in the manufacture of machine components and structural columns such as pipes, shafts, spacers, sprocket assemblies, mounting plates, spindles, axles, bolts, fixtures, mounting etc. and for utilization in industrial and domestic environments. These environments which includes automobile, construction, chemical processing, desalination, petrochemical, mining and extraction, energy generation, fertilizer and assembly plants exposes them to the electrochemical action of reactive anions which negatively impacts their operational life-span [1,2]. The low cost, recyclability, availability and rework-able mechanical and physical attributes of carbon steels accounts for their high volume usage worldwide compared to other steels (stainless steel, nickel alloys etc.) [3]. Carbon steels are generally made up ferrite i.e. carbon in solid solution phase diffused in α-iron [4]. The lack of passivating elements within their metallurgical structure exposes carbon steels to the growth of porous oxide on its surface which gradually degenerates the steels over time and renders its useless. This phenomenon is known as corrosion. It is the degeneration of a metallic material and/or its mechanical and physical properties due to the electrochemical interactions/reactions with their environment [5,6]. The collateral damage resulting from corrosion process is generally huge resulting in cost overheads due to sustenance, repair and substitution of degraded components and corrosion mitigation. To countered this problem, a number of surface modification techniques such as cathodic protection, anodizing, electrodeposition, chrome plating, electroplating, anodic protection, application of highly resistant stainless steels and paint coating have been developed over the years [7,8]. However, they have been proven to be costly, design specific and cannot be universally applied [9–11]. Utilization of corrosion inhibitors has been tested and confirmed to be the most unchallenging and affordable technique for corrosion control [12,13]. Corrosion inhibitors are fluid derivatives that significantly reduces or completely stifles the electrochemical reactions responsible for surface degradation of metallic alloys [14]. Their application tends to be widespread across most sectors ranging from petrochemicals to automobiles. Most effective traditional corrosion inhibitors such as nitrite, chromate, and phosphate are inorganic derivatives and tends to be harmful to personnel, unsustainable to the ecosystem and subject to restrictive government policies limiting their usage [15]. Corrosion inhibitors from carbon-based derivatives are also potent but similarly hazardous. Their performance is subject to their basic elemental composition, chemical structure and physicochemical properties [16–18]. Corrosion inhibitors are conventionally listed as vapour phase, cathodic, passivating, anodic, organic or mixed-type with regards to mechanism of inhibition. Some inhibitors influence the corrosion potential of the metallic alloys under study while others form protective film over the alloy [19]. The protective film interacts with the metallic surface through passivation, precipitation or adsorption [20]. Currently, research to incorporate green compounds as metallic corrosion inhibitors is ongoing globally to replace their toxic counterparts. However, there are challenges to overcome and inhibition mechanism established such as their reactive nature and solubility. Green chemical compounds have phytochemical properties and are environmentally sustainable, non-toxic, economical and gotten majorly from plant concentrates. Previous research experimentation on plant concentrates for assessment of their corrosion inhibition properties has yielded important data. However, the validity of the data output is hampered by the limited shelf-life and weak adsorption properties of the concentrates [21–25]. Research on essential oil concentrates is ongoing with mixed results. Further study is needed to establish their corrosion inhibition properties [26–35]. Pelargonium is a genus of plant consisting of about 280 species [36,37]. They are evergreen perennials indigenous to warm temperate and tropical regions of the world. Their application ranges from ornamental plants to their use in the perfume industry due to their scents and in herbal medicine [38,39]. Citrus recticulata is used in the food industry as seasoning for used in salads, desserts and main dishes [40]. Fresh citrus recticulata juice and frozen juice concentrate are also available. In medicine, the dried peel of the fruit is used in regulation of ch'i and to enhance digestion [41]. The corrosion inhibition property of Pelargonium was tested on mild steel in HCl solution. Results showed it performed effectively [42]. Research has shown that Citrus recticulate effectively inhibited the corrosion of Cu and Al in NaOH solution [43,44]. This article studies the inhibition performance and protection efficiency of *Pelargonium, Citrus reticulata* oil concentrates and their admixture on the degeneration of 1018 carbon steel in intermediate strength H_2SO_4 and HCl media.

2. Experimental methods

2.1. Materials

1018 carbon steel (18CS) specimens of columnar dimension (diameter 1.2 cm) with nominal weight constituent (%) consisting of 0.7% Mn, 0.15% C, 0.06% S, 0.04% P and 99.06% Fe after characterization with Jeol scanning electron microscope at the Central Lab., Covenant University, Ota, Ogun State, Nigeria. 18CS specimens were prepared with high speed steel cutting machine into specimens with mean dimensions of 1 cm for coupon measurement. Specimens for electrochemical polarization and potential-time evaluation were attached to a Cu wire with soldering iron before being mounted in acrylic resin mounts. The visible morphology of the steel abraded with sandpapers (60, 120, 320, 400, 600, 1500 and 2000 grits) and burnished with 6 μm diamond fluid prior to decontamination with bi-distilled H_2O and propanone. *Pelargonium* (Pe) and *Citrus reticulata* (Cr) essential oil was procured from NOW Foods, USA, and formulated in cubic concentrates of 0%, 1%, 1.5%, 2%, 2.5%, 3% and 3.5% respectively per 200 ml of 0.5M H_2SO_4 and HCl solutions The concentrates were

combined (PeCr) in ratio 1:1 and also formulated in cubic concentrates of 0%, 1%, 1.5%, 2%, 2.5%, 3% and 3.5% respectively per 200 ml of the acid electrolytes.

2.2. Electrochemical polarization and open circuit potential evaluation

Electrochemical evaluation was conducted at 35 °C steady temperature utilizing a multicomponent electrode setup inserted into a holding beaker (saturated with the acid-concentrate media) and plugged to the potentiostat (Digi-Ivy 2311) and computer system. They electrodes are 1018CS sample electrodes with exterior morphology of 1.126 cm^3, Ag/AgCl standard electrode and Pt rod auxillary electrode. Polarization curves were plotted at 0.00145 V/s (scan rate) from −1.1 V and +1.65 V. Corrosion current density C_J, (A/cm^2) and corrosion potential, C_p (V) values were computed by Tafel derivation. Corrosion rate, C_t (mm/y) was enumerated from the mathematical representation below;

$$C_R = \frac{0.00327 \times C_J \times E_q}{d} \quad (1)$$

where C_q represents the correlative weight (g) of alloy, 0.00327 stands for corrosion rate constant and d represents density (g/cm^3). Protection performance (inhibition efficiency), ξ_F (%) was enumerated from the mathematical representation below;

$$\xi_F = \left[1 - \left(\frac{C_{R2}}{C_{R1}}\right)\right] \times 100 \quad (2)$$

C_{R1} and C_{R2} represents weight loss values without and with the concentrates. Polarization resistance, R_p, (Ω) was computed as displayed below;

$$R_p = 2.303 \frac{B_a B_c}{B_a + B_c}\left(\frac{1}{I_{cr}}\right) \quad (3)$$

B_a and B_c represents anodic and cathodic Tafel slopes (V/dec).

2.3. ATF-FTIR spectroscopy and optical image assessment

1% Pe concentration/0.5 M H_2SO_4 and HCl media, 1% Cr concentration/0.5 M H_2SO_4 and HCl media and 1% PeCr concentration/0.5 M H_2SO_4 and HCl media preceding and following corrosion evaluation were studied using infrared rays with Bruker Alpha FTIR instrument spectrometer within the wavelength span of 375–7500 cm^{-1}, and accuracy of 0.9 cm^{-1}. The spectral patterns were evaluated and compared to the standardized ATF-FTIR Table for determination of reactive groups involved in the suppression of the redox reaction mechanism. Optical image characterization of 1018CS specimens prior to and after corrosion test in the electrolyte with and without the presence of the concentrates was performed with USB digital microscope.

2.4. X-ray diffractommetry

X-ray diffraction plots and pattern list of the phase compounds, precipitates and metallic complexes on 18CS surface in the presence of and without the oil concentrates were produced after analysis with Bruker AXS D2 phaser powder diffractometer using single chromatic CuKα energy which was released at 30 kV and 10 mA, at step dimension of 0.03° in 2θ. The scan software is the conventional scan exccelerator. Phases were revealed using X'Pert Highscore plus program at the University of Johannesburg, South Africa.

2.5. Coupon measurement

18CS steel specimens were firstly weighed and individually submerged in 200 ml of the acid-concentrate electrolyte for 288 h. Weight measurement was done at 24 h interlude. Corrosion rate, C_t (mm/y) was computed as follows;

$$C_t = \left[\frac{87.6\omega}{DAt}\right] \quad (4)$$

ω represents weight loss (g), D represents density (g/cm^3), A illustrates overall exterior morphology of the 1018CS sample (cm^2) and 87.6 represents corrosion rate constant. t represents time (h). Inhibition performance (η) was assessed from the numerical relationship below;

$$\eta = \left[\frac{\omega_1 - \omega_2}{\omega_1}\right] \times 100 \quad (5)$$

ω_1 and ω_2 represents weight variation at specific oil concentrate concentrations.

3. Results and discussion

3.1. Electrochemical polarization evaluation

Corrosion polarization behaviour of 18CS in 0.5 M H_2SO_4 and HCl solution was studied at specific concentrations (0%–3.5%) of Pe, Cr and PeCr essential oil concentrates. The potentiodynamic polarization plots for 18CS in the acid electrolyte with and without the inhibitors are revealed from Fig. 1(a) to Fig. 3(b). Fig. 1(a) and (b) reveals the plots of 18CS in H_2SO_4 and HCl solutions at 0%–3.5% Pe concentrate. Fig. 2(a) and (b) reveals the plots of 18CS in H_2SO_4 and HCl solutions at 0%–3.5% Cr. Fig. 3(a) and (b) presents the plots of 18CS in H_2SO_4 and HCl solutions at 0%–3.5% PeCr. Tables 1–3 shows the polarization data retrieved from the plots. Generally, the polarization plots from Figs. 1(a)–3(b) depict the substantial variation between the plots at 0% concentrate concentration and the plots at specific (1%–3.5%) concentrate concentration. This is by reason of the degree of redox reaction processes taking place on the surface of 18CS in the absence of the concentrates during potential scanning. 18CS undergoes oxidation whereby it losses electrons and discharges into the electrolyte as ionized metallic elements. Simultaneously, O_2 reduction and H_2 evolution reaction occurs resulting in the evolution of H_2 gas [45]. In the presence of Pe concentrate in H_2SO_4 and HCl solution, significant decrease in the cathodic-anodic polarization slopes are visible [Fig. 1(a) and (b)]. This is due to the reduction of the redox reactions by protonated concentrate species [46]. Examination of Table 1 reveals the substantial contrast in corrosion rate outcomes of 18CS at 0% Pe concentration (4.833 mm/y and 3.635 mm/y) and at specific Pe concentration in both acids. 18CS corrosion rate outcomes

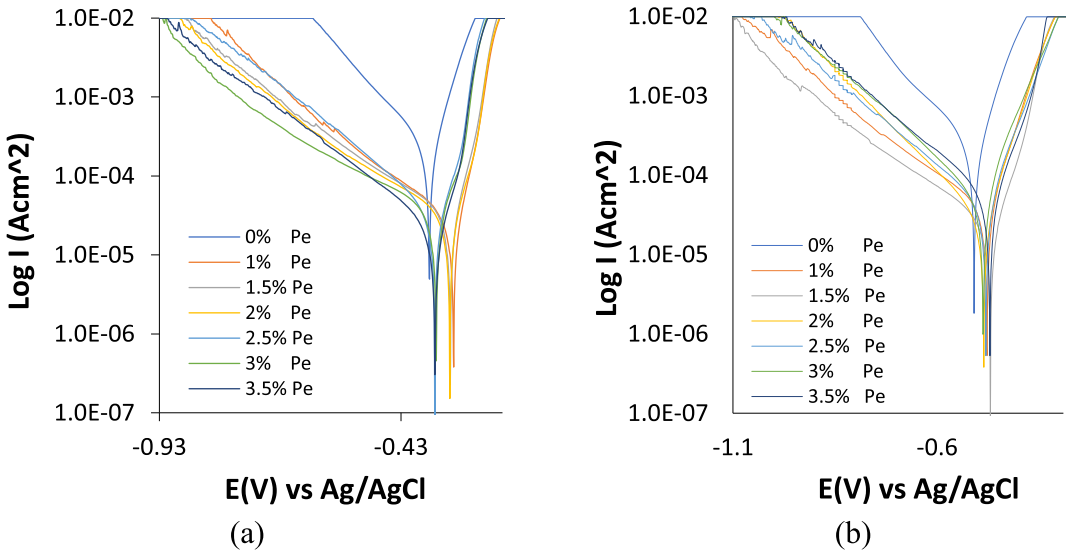

Fig. 1 – Electrochemical plots of 18CS in (a) H_2SO_4 solution and (b) HCl media at specific concentrations of Pe concentrate (0%–3.5% concentration).

with Pe concentrate ranges from 2.549 mm/y and 0.741 mm/y at 1% Pe to 0.408 mm/y and 0.887 mm/y at 3.5% Pe. The values correspond to and are analogous to the corrosion current density. The generally higher corrosion rate values in H_2SO_4 compared to HCl is by reason of the diprotic nature of H_2SO_4 acid whereby it ionizes in H_2O at higher dissociation constant compared to HCl. The corresponding inhibition efficiency values shows performance of Pe in H_2SO_4 is directly proportional to Pe concentration. Effective inhibition effect on 18CS was attained at 3% Pe concentration in H_2SO_4, whereby in HCl effective inhibition occurred at all Pe concentrations signifying performance non-dependent on its concentration.

With Cr concentrate, corrosion rate of 18CS significantly reduced compared to its value at 0% Cr concentration. The corresponding inhibition efficiency values in both acid indicates effective corrosion inhibition at all concentrations and 74.72% and 78.12% in H_2SO_4, 78.74% and 77.85% in HCl. These values indicate thermodynamic stability of the Cr concentrate molecules within both electrolytes in interaction with 18CS surface. The contrast in the corrosion potential of the graphs in Fig. 2(a) shows substantial shift to cathodic values relative to the potential at 0% Cr concentration. The optimal variation is 0.115 V indicating cathodic inhibition behaviour of Cr in H_2SO_4 solution (Table 2). This statement is also confirmed from the disproportionate decrease in cathodic slope with respect to increase in Cr concentration. In HCl solution, Cr exhibited mixed inhibition properties from observation of the potential of its cathodic-anodic polarization plots. The

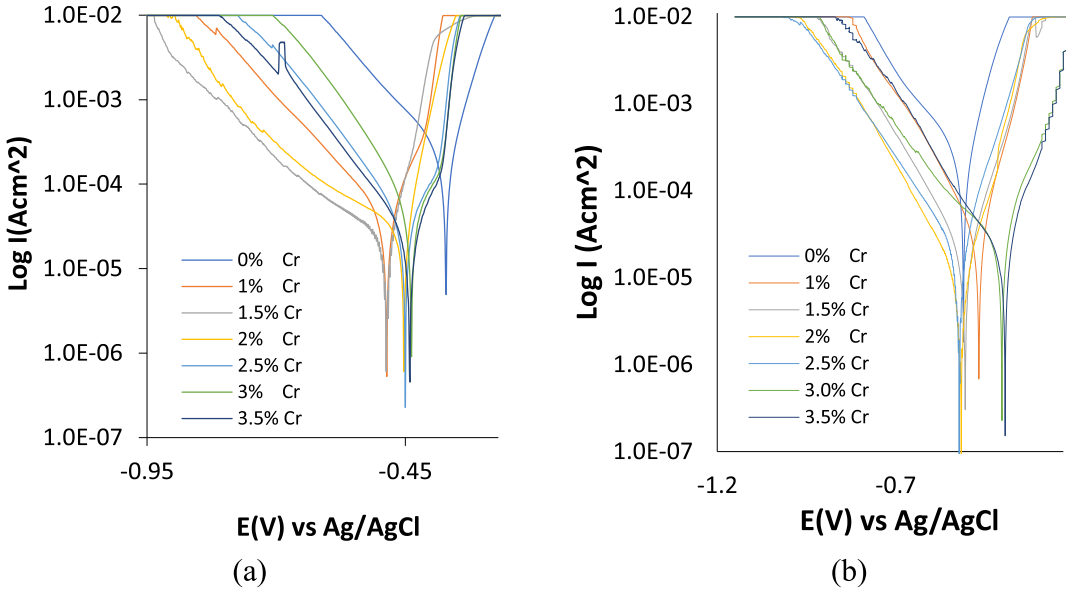

Fig. 2 – Electrochemical plots of 18CS in (a) H_2SO_4 solution and (b) HCl media at specific concentrations of Cr concentrate (0%–3.5% concentration).

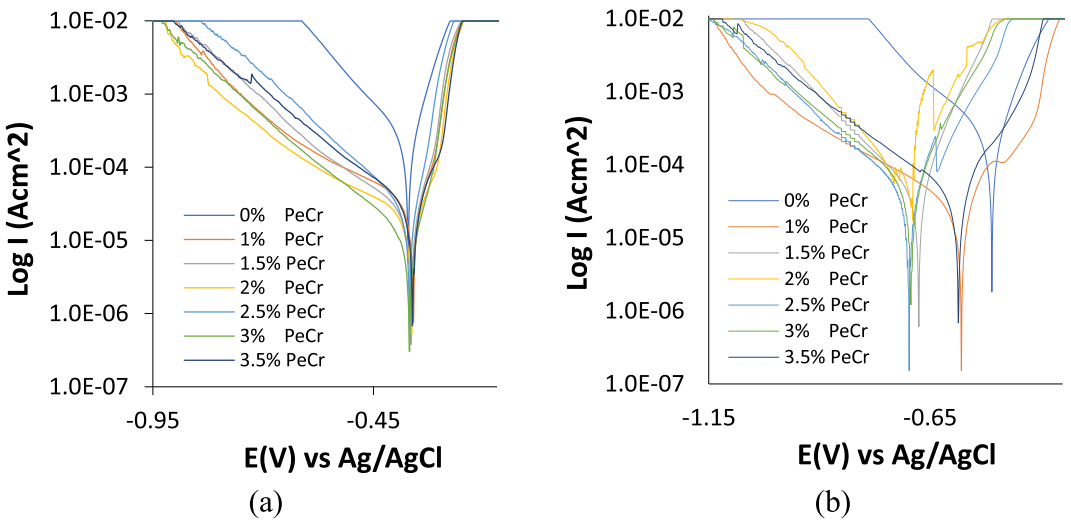

Fig. 3 – Electrochemical plots of 18CS in (a) H_2SO_4 solution and (b) HCl media at specific concentrations of PeCr concentrate (0%–3.5% concentration).

optimal variation of its polarization plots from the potential at 0% Cr concentration is less than 0.085V [47,48]. Comparing this to the performance of Pe concentrate on 18CS, Pe demonstrated dominant anodic inhibition properties in H_2SO_4 and cathodic protection effect in HCl. However, the optimal corrosion potential variation is less than 0.085 V; thus it is a dual-type inhibitor. The plot configuration of 18CS in the presence of Pe concentrate in H_2SO_4 and HCl solution significantly differs from its Cr counterpart. The plot configuration indicates activation control mechanisms dominates the inhibition reaction processes compared to Cr where surface coverage of MS surface strongly influences its inhibition mechanism.

The synergistic effect of Pe and Cr concentrate (PeCr) significantly enhanced the corrosion resistance of 18CS in HCl media due to stabilization of the adsorbed inhibitor cations [49,50]. In HCl solution, PeCr performance increased to outcomes between 82.80 mm/y and 95.46 mm/y due to strong attachment of inhibitor species on 18CS and significant lateral attraction effect among the concentrate species/molecules. The combined molecules of Pe and Cr molecular species stifled the diffusion of Cl-anions to the steel surface. This is aided by strong lateral attraction among the molecules. The performance of PeCr is significantly lower than the individual performance of the concentrates in H_2SO_4 solution. In H_2SO_4 solution, adsorption of the inhibitor species is weakened by the lateral repulsion effect among reacting concentrate species resulting in degradation rate outputs between 60.02 mm/y and 61.69 mm/y [51]. PeCr concentrates exhibited mixed type inhibition effect from inspection of the corrosion potential outputs analogous the corrosion potential at 0% inhibitor concentration. The cathodic-anodic polarization plots in

Table 1 – Electrochemical data for 18CS in H_2SO_4 and HCl media at specific concentrations of Pe concentrate (0%–3.5% concentration).

H_2SO_4 Solution									
Sample	Pe Conc. (%)	18CS C_t (mm/y)	Pe ξF (%)	C_I (A)	C_{Jd} (A/cm^2)	C_{Pt} (V)	P_r (Ω)	B_c (V/dec)	B_a (V/dec)
A	0	4.833	0	3.25E-04	3.68E-04	−0.371	79.09	−6.317	17.250
B	1	2.549	47.26	1.71E-04	1.94E-04	−0.321	104.34	−4.344	33.330
C	1.5	2.172	55.04	1.46E-04	1.66E-04	−0.328	257.90	−3.877	37.290
D	2	1.929	60.08	1.30E-04	1.47E-04	−0.329	347.40	−3.877	39.950
E	2.5	1.821	62.33	1.22E-04	1.39E-04	−0.360	356.00	−5.652	41.340
F	3	0.633	86.90	4.26E-05	4.82E-05	−0.357	1403.60	−3.576	41.930
G	3.5	0.408	91.56	2.74E-05	3.11E-05	−0.360	1937.10	−5.344	40.020
HCl Solution									
Sample	Pe Conc. (%)	18CS C_t (mm/y)	Pe ξF (%)	C_I (A)	C_{Jd} (A/cm^2)	C_{Pt} (V)	P_r (Ω)	B_c (V/dec)	B_a (V/dec)
A	0	3.635	0	2.44E-04	2.77E-04	−0.510	105.10	−5.583	14.670
B	1	0.741	79.62	4.98E-05	5.64E-05	−0.537	849.00	−4.181	16.640
C	1.5	0.586	83.89	3.94E-05	4.46E-05	−0.469	1012.00	−4.511	18.530
D	2	0.465	87.21	3.13E-05	3.54E-05	−0.485	1342.70	−5.945	15.340
E	2.5	0.461	87.32	3.10E-05	3.51E-05	−0.480	1305.60	−5.081	12.540
F	3	0.463	87.27	3.11E-05	3.52E-05	−0.487	1337.60	−5.570	12.000
G	3.5	0.887	75.60	5.96E-05	6.76E-05	−0.470	809.30	−5.242	14.290

Table 2 – Electrochemical data for 18CS in H_2SO_4 and HCl media at specific concentrations of Cr concentrate (0%–3.5% concentration).

H_2SO_4 Solution									
Sample	Cr Conc. (%)	18CS C_t (mm/y)	Pe ξF (%)	C_I (A)	C_{Jd} (A/cm^2)	C_{Pt} (V)	P_r (Ω)	B_c (V/dec)	B_a (V/dec)
A	0	4.833	0	3.25E-04	3.68E-04	−0.371	79.09	−6.317	17.250
B	1	1.221	74.72	8.21E-05	9.31E-05	−0.486	413.60	−6.743	27.510
C	1.5	1.310	72.89	8.81E-05	9.98E-05	−0.487	629.40	−3.808	33.310
D	2	1.422	70.57	9.56E-05	1.08E-04	−0.453	458.50	−3.391	24.130
E	2.5	1.119	76.85	7.52E-05	8.52E-05	−0.450	492.90	−8.667	50.620
F	3	1.176	75.67	7.90E-05	8.96E-05	−0.438	364.80	−9.930	54.550
G	3.5	1.057	78.12	7.11E-05	8.05E-05	−0.441	682.90	−7.802	53.820
HCl Solution									
Sample	Cr Conc. (%)	18CS C_t (mm/y)	Pe ξF (%)	C_I (A)	C_{Jd} (A/cm^2)	C_{Pt} (V)	P_r (Ω)	B_c (V/dec)	B_a (V/dec)
A	0	3.635	0	2.44E-04	2.77E-04	−0.510	105.10	−5.583	14.670
B	1	0.773	78.74	5.20E-05	5.89E-05	−0.467	612.40	−8.029	14.850
C	1.5	0.741	79.61	4.98E-05	5.65E-05	−0.505	1176.00	−7.675	12.540
D	2	0.296	91.87	1.99E-05	2.25E-05	−0.516	2672.00	−7.239	12.370
E	2.5	0.686	81.12	4.62E-05	5.23E-05	−0.522	1342.00	−6.734	12.410
F	3	0.740	79.64	4.98E-05	5.64E-05	−0.516	960.20	−11.560	14.880
G	3.5	0.805	77.85	5.41E-05	6.14E-05	−0.526	913.00	−8.645	14.010

Table 3 – Electrochemical data for 18CS in H_2SO_4 and HCl media at specific concentrations of PeCr concentrate (0%–3.5% concentration).

H_2SO_4 Solution									
Sample	PeCr Conc. (%)	18CS C_t (mm/y)	Pe ξF (%)	C_I (A)	C_{Jd} (A/cm^2)	C_{Pt} (V)	P_r (Ω)	B_c (V/dec)	B_a (V/dec)
A	0	4.833	0	3.25E-04	3.68E-04	−0.371	79.09	−6.317	17.250
B	1	1.932	60.02	1.30E-04	1.47E-04	−0.360	644.30	−3.505	36.760
C	1.5	1.811	62.52	1.22E-04	1.38E-04	−0.365	808.40	−4.285	38.200
D	2	1.725	64.30	1.16E-04	1.31E-04	−0.363	988.50	−3.232	46.370
E	2.5	1.919	60.29	1.29E-04	1.46E-04	−0.368	658.20	−6.108	26.060
F	3	1.567	67.58	1.05E-04	1.19E-04	−0.368	677.00	−5.288	40.570
G	3.5	1.851	61.69	1.24E-04	1.41E-04	−0.362	745.50	−4.514	41.870
HCl Solution									
Sample	PeCr Conc. (%)	18CS C_t (mm/y)	Pe ξF (%)	C_I (A)	C_{Jd} (A/cm^2)	C_{Pt} (V)	P_r (Ω)	B_c (V/dec)	B_a (V/dec)
A	0	3.635	0	2.44E-04	2.77E-04	−0.510	105.10	−5.583	14.670
B	1	0.625	82.80	4.20E-05	4.76E-05	−0.472	414.20	−4.892	14.340
C	1.5	0.359	90.12	2.42E-05	2.74E-05	−0.475	457.60	−6.136	14.290
D	2	0.248	93.19	1.66E-05	1.89E-05	−0.489	47.90	−8.934	13.260
E	2.5	0.369	89.85	2.48E-05	2.81E-05	−0.497	645.40	−5.542	12.226
F	3	0.352	90.33	2.36E-05	2.68E-05	−0.493	507.40	−5.479	10.090
G	3.5	0.165	95.46	1.11E-05	1.26E-05	−0.496	1066.00	−7.446	13.650

Table 4 – Coupon measurement data for 18CS in H_2SO_4 and HCl media (0%–3.5% Pe and Cr concentrate concentration) at 288 h.

18CS Sample	Pe Concentrate Conc. (%)	Pe/H_2SO_4		Pe/HCl		Cr/H_2SO_4		Cr/HCl	
		Corrosion Rt. (mm/y)	Inhibition Eff. (%)	Corrosion Rt. (mm/y)	Inhibition Eff. (%)	Corrosion Rt. (mm/y)	Inhibition Eff. (%)	Corrosion Rt. (mm/y)	Inhibition Eff. (%)
A	0	39.744	–	14.853	–	42.030	–	12.665	–
B	1	21.182	46.70	3.510	76.37	16.688	60.29	2.868	77.35
C	1.5	17.829	55.14	5.633	62.08	12.651	69.90	2.780	78.05
D	2	16.151	59.36	1.625	89.06	20.295	51.71	1.780	85.94
E	2.5	15.397	61.26	5.179	65.13	13.661	67.50	2.648	79.09
F	3	1.521	96.17	1.532	89.68	14.334	65.90	2.713	78.58
G	3.5	1.803	95.46	3.976	73.23	11.310	73.09	3.264	74.23

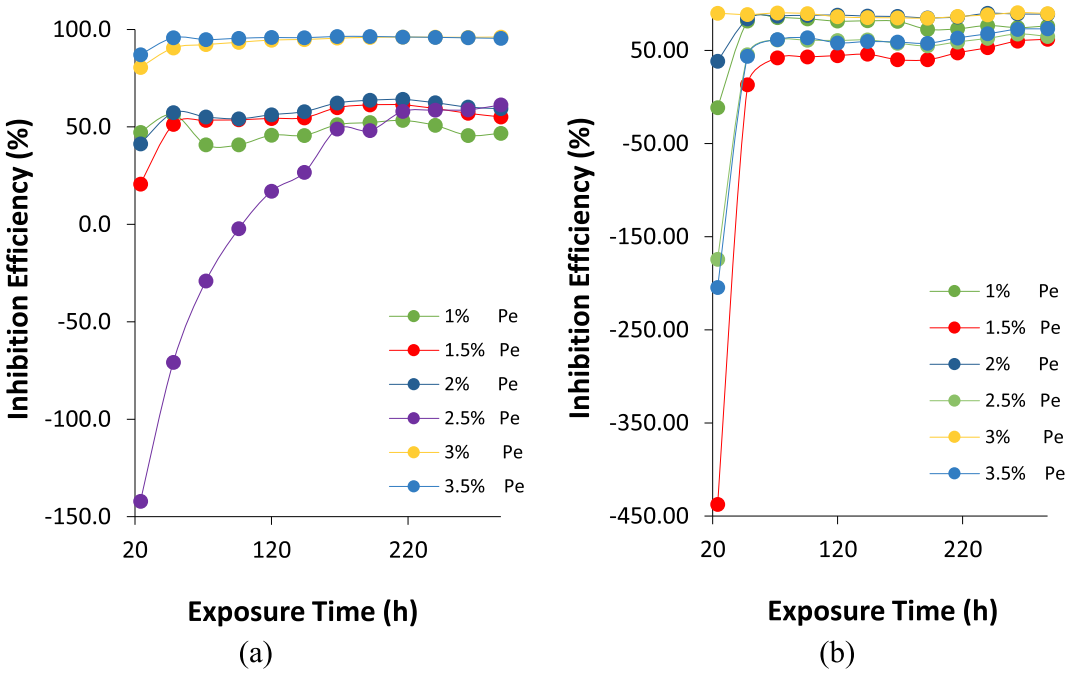

Fig. 4 – Plots of Pe concentrate inhibition efficiency to exposure from (a) H_2SO_4 media and (b) HCl media.

Fig. 3(a) and (b) differs from each other due to the influence of PeCr on the polarization behaviour and by extension the redox reaction processes. The substantial difference of the anodic polarization plots in Fig. 3(b) signifies suppression of the oxidation half–cell reactions whereby surface coverage of 18CS restricts the diffusion of the destructive anions to the steel exterior. Secondly, electrostatic attraction between the concentrate molecules and 18CS surface displaces the adsorption of O_2 atoms to the steel surface. In Fig. 3(a), the anodic reaction processes appear under activation control. The corrosion potential in Table 3 depict significant shift to anodic potentials signifying dominant anodic reaction and inhibition processes. It must be noted that the high cathodic and anodic Tafel slope values is due to their low exchange current densities at equilibrium potential. The exchange current density indicates the rate of oxidation and reduction reactions at the electrode. The lower the exchange current density, the slower the redox electrochemical reaction. Hence, the values in the manuscript tables shows the presence of the inhibitors significantly reduced the oxidation half–cell

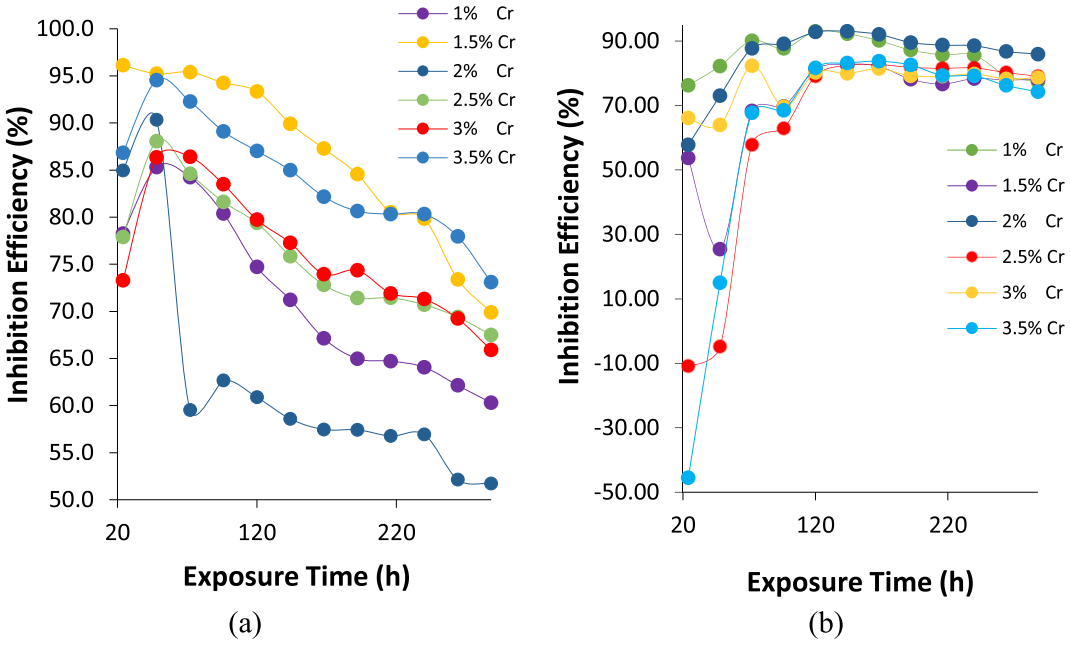

Fig. 5 – Plots of Cr concentrate inhibition efficiency to exposure from (a) H_2SO_4 solution and (b) HCl solution.

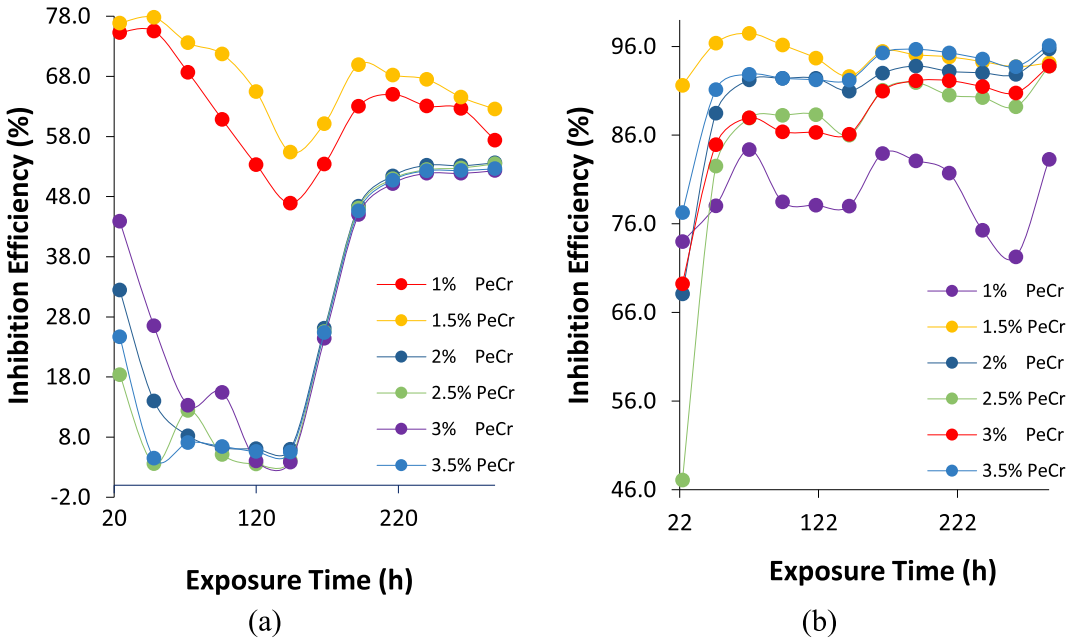

Fig. 6 – Plots of PeCr concentrate inhibition efficiency to exposure from (a) H_2SO_4 media and (b) HCl media.

reactions compared to the cathodic counterpart. While the values may be generally high, it is due to hysteresis in electrochemical reactions at molecular and atomic level which invariably are strongly dependent on the composition of the metal/alloy the acid solution, the concentration of the soluble

7–9(c) depict the representative optical images of 18CS prior to corrosion, following corrosion at 1% concentrate concentration and after corrosion at 3.5% concentrate concentration from H_2SO_4 and HCl solution. Inspection of Table 4 shows Pe concentrate performed poorly in H_2SO_4 solution from 1% to

Table 5 – Coupon measurement data for 18CS in H_2SO_4 and HCl media (0%–3.5% PeCr concentrate concentration) at 288 h.

18CS Sample	Pe Concentrate Conc. (%)	PeCr/H_2SO_4		PeCr/HCl	
		Corrosion Rt. (mm/y)	Inhibition Eff. (%)	Corrosion Rt. (mm/y)	Inhibition Eff. (%)
A	0	49.985	–	31.200	–
B	1	21.300	57.39	5.211	83.30
C	1.5	18.728	62.53	1.825	94.15
D	2	23.187	53.61	1.329	95.74
E	2.5	23.264	53.46	1.936	93.79
F	3	23.837	52.31	1.930	93.81
G	3.5	23.679	52.63	1.208	96.13

species.

3.2. *Coupon measurement and optimal microscopy studies*

18CS coupons were immersed in H_2SO_4 and HCl media for 288 h amidst and without specific concentrations of Pe, Cr and PeCr concentrates. Plots of the concentrate inhibition efficiencies against exposure time were produced. Corrosion rate and inhibition efficiency data for the concentrates with respect to their performance at 288 h are exhibited in Tables 4 and 5. Fig. 4(a) and (b) illustrates the inhibition efficiency plots of Pe concentrate against exposure time in H_2SO_4 and HCl media, Fig. 5(a) and (b) depict the plots of Cr concentrate against exposure time in H_2SO_4 4 and HCl media. Fig. 6(a) and (b) displays the plots of PeCr against exposure time. Figs.

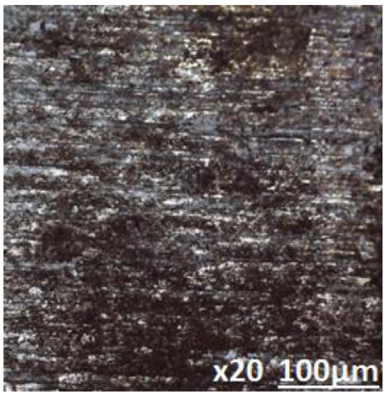

Fig. 7 – Optical representation of 18CS prior to corrosion test.

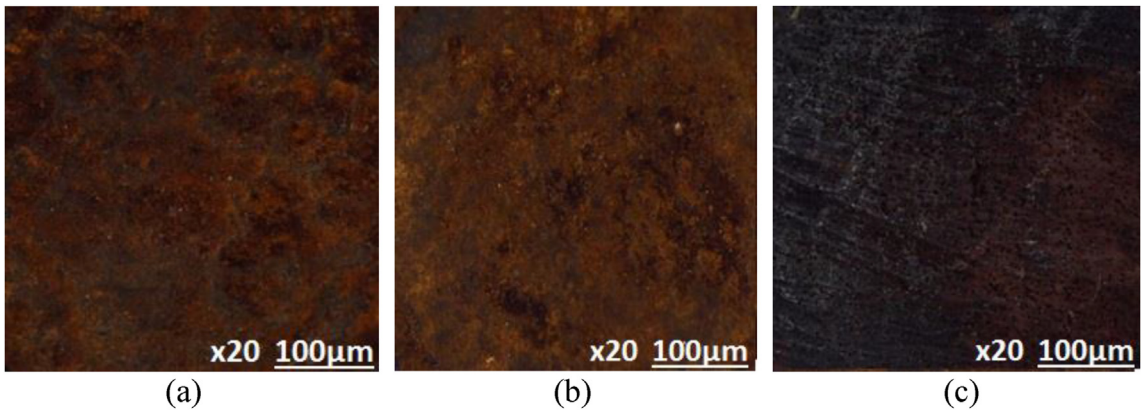

Fig. 8 – Optical representative image of 18CS from H_2SO_4 media at (a) 0%, (b) 1% and (c) 3.5% concentrate concentration.

2.5% Pe concentration (inhibition efficiency between 46.70% and 61.26%). However, from 3% Pe concentration inhibition efficiency has significantly increased to 96.17%, culminating at 95.46% at 3.5% Pe concentration. This observation contrasts the performance of Pe concentrate in HCl solution where relative stability in inhibition performance was observed. The inhibition values ranges between 76.37% and 73.23% (from 1% to 3.5% Pe concentration). The plots in Fig. 4 gives a clearer view of the performance of Pe concentrate where Pe inhibition performance significantly varies with time and concentration in H_2SO_4 in comparison to its performance in HCl solution [52].

The performance of Cr concentrate in HCl (Table 4) were generally similar to Pe in HCl. Cr inhibition efficiency varies from 77.35% at 1% Cr concentration to 74.23% at 3.5% Cr concentration. The plot configuration [Fig. 5(b)] showed Cr concentrate attained relative stability in HCl at 120 h compared to Pe in HCl at 72 h. Cr performance in H_2SO_4 is not recommended for industrial application as its inhibition performance decreased with time [Fig. 5(a)] and culminating at the final values shown in Table 4 at 288 h [53]. This observation is probably due to the diprotic nature of H_2SO_4 anion whereby its ionization in H_2O is much stronger than the corresponding ionization of HCl due to its of two H^+ atoms. HCl is monoprotic in nature with weaker ionization potential in H_2O compared to H_2SO_4. Hence, the SO_4^{2-} anion tends to be more aggressive to the steel surface and more resistant to the electrochemical action of the inhibitors. Although Cr inhibition efficiency at 3.5% concentration is 73.09%, it is a result in substantive decrease with respect to exposure time. Admixture of Cr and Pe concentrates (PeCr) did not offer any advantage in inhibition performance in H_2SO_4 solution as the inhibition efficiency of PeCr with respect to concentration shown in Table 5 were all below 60%. The corresponding plot configuration [Fig. 6(a)] depicts an unstable compound with poor inhibition effect. However, in HCl solution, PeCr protected 18CS more effectively than the individual performance of Cr and Pe concentrates. Inhibition efficiency ranged from 83.30% at 1% PeCr concentration to 96.13% at 3.5% PeCr concentration; though the plot configuration in Fig. 6(b) shows PeCr performance varies significantly with time. i.e. thermodynamically unstable compared to the performance of Pe concentrate in HCl after 72 h of exposure [Fig. 5(b)]. The optical image in Fig. 7 depict the morphology of 18CS preceding corrosion test. Figs. 8(a) and 9(a) depict the surface of 18CS prior to corrosion in H_2SO_4 and HCl solutions. The surfaces depict severe surface degradation compared to Fig. 7. Corrosion pits are identified in Fig. 9(a) on account of the localized reactive nature of Cl^- anions in HCl in comparison to general surface deterioration in Fig. 8(a) [54]. The representations in Figs. 8(b) and 9(b) shows the surface of 18CS from the weakest concentrate concentration. At the weakest concentrate concentration, the extent of surface degradation is almost similar to the morphology of

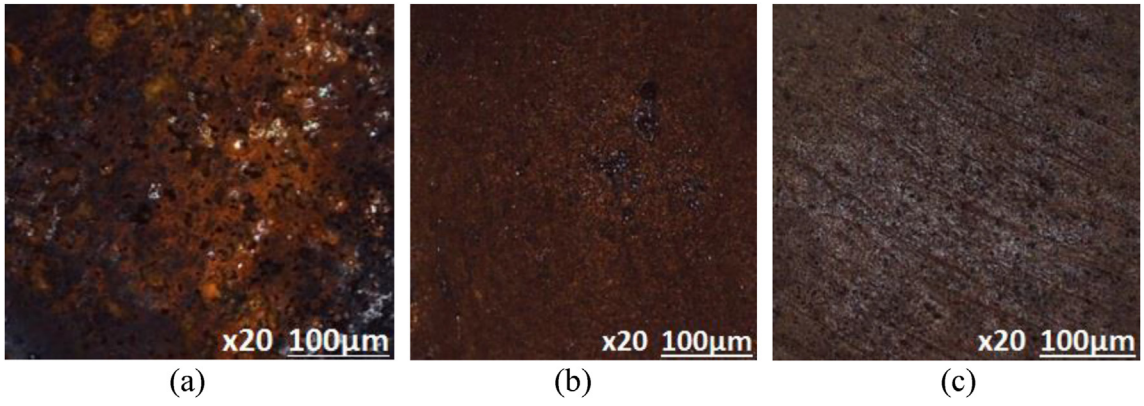

Fig. 9 – Optical representative image of 18CS from HCl media at (a) 0%, (b) 1% and (c) 3.5% concentrate concentration.

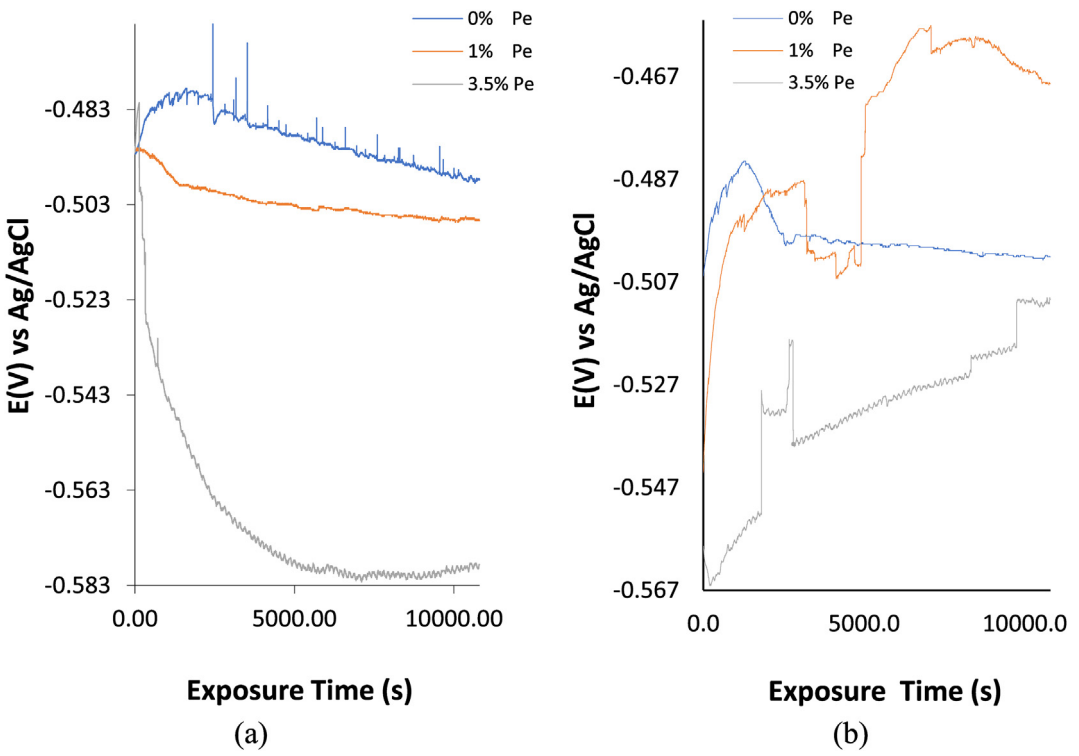

Fig. 10 – OCP plots of 18CS at 0%, 1% and 3.5% Pe concentration in (a) H_2SO_4 media and (b) HCl media.

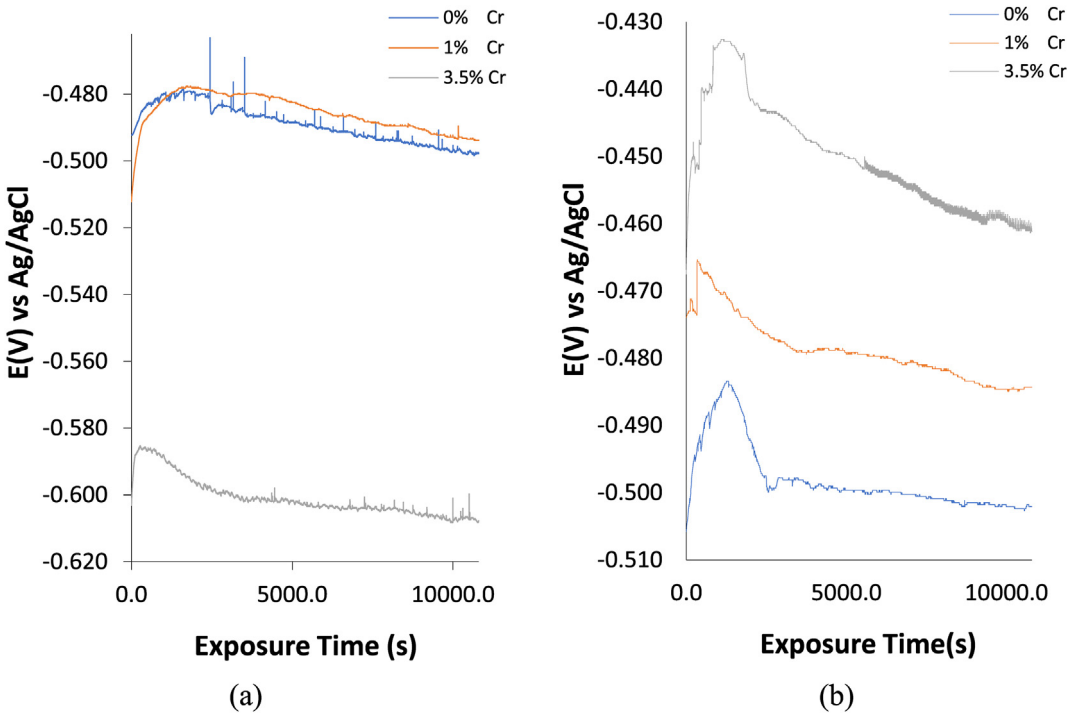

Fig. 11 – OCP plots of 18CS at 0%, 1% and 3.5% Cr concentration in (a) H_2SO_4 media and (b) HCl media.

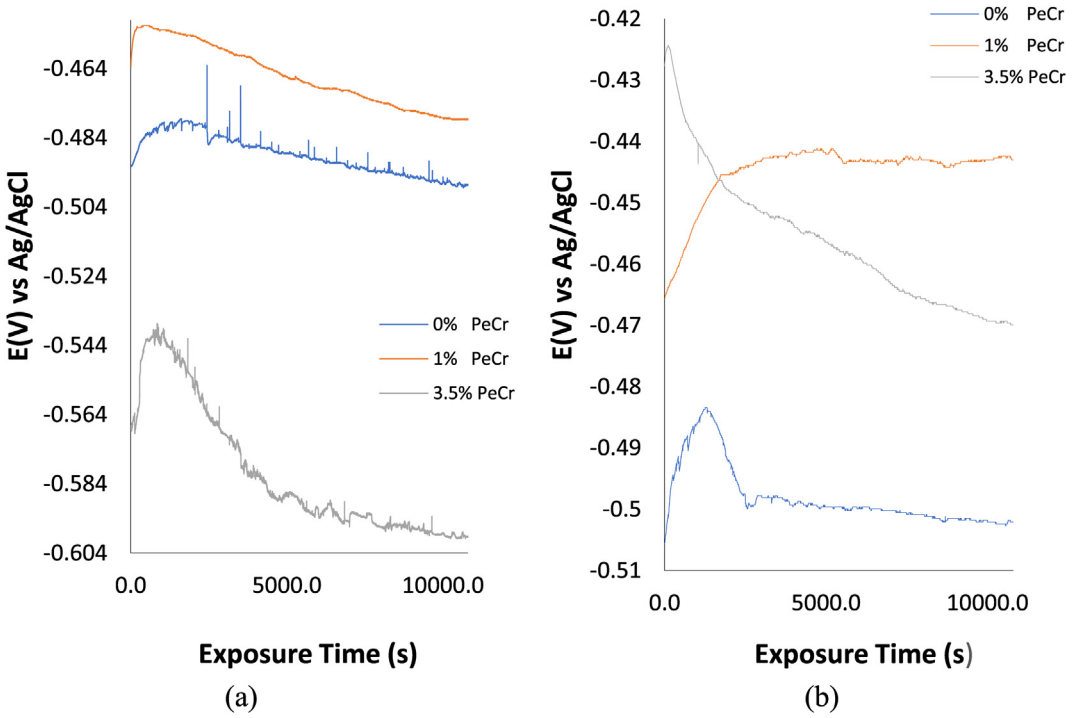

Fig. 12 – OCP plots of 18CS at 0%, 1% and 3.5% PeCr concentration in (a) H_2SO_4 media and (b) HCl media.

18CS at 0% concentrate concentration. However, the morphologies shown in Figs. 8(c) and 9(c) depict effective concentrate protection of 18CS surface despite minor surface deterioration compared to Fig. 7. The minor deterioration is by reason of the time-dependent effect of the concentrates as displayed in the plot configurations of concentrate concentration versus exposure time (inhibition efficiency plots).

3.3. *Potential-time evaluation*

Potential-time evaluation of 18CS in H_2SO_4 and HCl media at 0%, 1% and 3.5% Pe, Cr and PeCr concentrate concentration was done to assess the thermodynamic stability, active–passive transition behaviour and corrosion tendency of 18CS in the acid-concentrate electrolyte. The OCP plots are

Table 6 – ATR-FTIR spectroscopic output at 1%Pe/0.5M H_2SO_4 and HCl media, preceding and following 18CS corrosion.

Pe H_2SO_4				
Standard wavenumber (cm^{-1})	Computed Wavenumber, preceding corrosion (cm^{-1})	Computed Wavenumber, after corrosion (cm^{-1})	Bond	Reactive Group
1760–1665	1708	–	C=O stretch	carbonyls (general), carboxylic acids, alpha-beta–unsaturated aldehydes, ketones
1650–1580	1590	1618	N–H bend, C–C stretch (in-ring)	primary amines, aromatics
1500–1400	1440	–	C–C stretch (in ring)	aromatics
1320–1000	1022	1060	C–O stretch, C–N stretch	alcohols, carboxylic acids, esters, ethers, aliphatic amines
Pe HCl				
Standard Wavenumber (cm^{-1})	Computed Wavenumber, preceding corrosion (cm^{-1})	Computed Wavenumber, after corrosion (cm^{-1})	Bond	Reactive Group
3330–2500	–	2926	O–H stretch, C–H stretch	carboxylic acids
1650–1580	–	1612	N–H bend	primary amines
1250–1020	1072	1066	C–N stretch	aliphatic amines

Table 7 – ATR-FTIR spectroscopic output at 1%Cr/0.5M H_2SO_4 and HCl solution, preceding and following 18CS corrosion.

Cr H_2SO_4				
Standard wavenumber (cm^{-1})	Computed Wavenumber, preceding corrosion (cm^{-1})	Computed Wavenumber, after corrosion (cm^{-1})	Bond	Reactive Group
1650–1580	1602	1586	N–H bend	primary amines
1370–1350	1380	1364	C–H rock	alkanes
1320–1000	1024	–	C–O stretch	alcohols, carboxylic acids, esters, ethers, aliphatic amines
Cr HCl				
Standard Wavenumber (cm^{-1})	Computed Wavenumber, preceding corrosion (cm^{-1})	Computed Wavenumber, after corrosion (cm^{-1})	Bond	Reactive Group
3500–3200	3462	–	O–H stretch, H-bonded	alcohols, phenols
1680–1640	1642	–	-C=C-stretch	alkenes
1650–1580	1642	1608	N–H bend	primary amines
1250–1020	1070	–	C–N stretch	aliphatic amines
910–665	790	–	N–H wag	primary, secondary amines
900–675			C–H "oop"	aromatics
850–550			C–Cl stretch	alkyl halides

displayed from Figs. 10(a)–12(b). Fig. 10(a) and (b) depict the plots of 18CS in H_2SO_4 and HCl media at calculated Pe concentration. Fig. 10(a) and (b) presents the plots of 18CS in H_2SO_4 and HCl solution at calculated Cr concentration, whereas Fig. 12(a) and (b) depict the plots of 18CS in H_2SO_4 and HCl media at specific PeCr concentration. Contrary to the

Table 8 – ATR-FTIR spectroscopic output at 1%PeCr/0.5M H_2SO_4 and HCl solution, preceding and following 18CS corrosion.

PeCr H_2SO_4				
Standard wavenumber (cm^{-1})	Computed Wavenumber, preceding corrosion (cm^{-1})	Computed Wavenumber, after corrosion (cm^{-1})	Bond	Reactive Group
3330–2500	–	2920	O–H stretch, C–H stretch	carboxylic acids, alkanes
1710–1665	–	1702	C=O stretch	alpha, beta–unsaturated aldehydes, ketones
1650–1580	–	1598	N–H bend, C–C stretch (in-ring)	primary amines, aromatics
1320–1000	1038	1030	C–O stretch, C–N stretch	alcohols, carboxylic acids, esters, ethers, aliphatic amines
PeCr HCl				
Standard Wavenumber (cm^{-1})	Computed Wavenumber, preceding corrosion (cm^{-1})	Computed Wavenumber, after corrosion (cm^{-1})	Bond	Reactive Group
3500–3200	3448	3446	O–H stretch, H-bonded	alcohols, phenols
3000–2850	2930	–	C–H stretch	alkanes
1650–1580	–	1610	N–H bend	primary amines
1250–1020	1068	–	C–N stretch	aliphatic amines
1300–1150			C–H wag (-CH_2X)	alkyl halides
1320–1000			C–O stretch	alcohols, carboxylic acids, esters, ethers
850–550	782	–	C–Cl stretch	alkyl halides
900–675			C–H "oop"	aromatics
910–665			N–H wag	

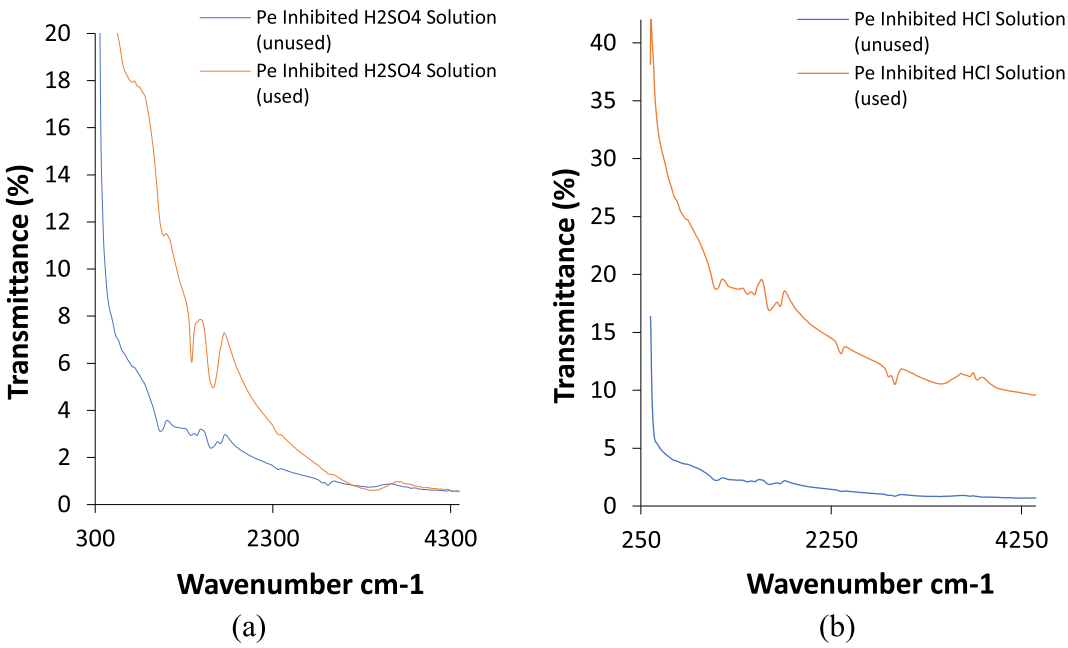

Fig. 13 – ATF-FTIR spectra plots of (a) 1% Pe/0.5M H_2SO_4 solution and (b) 1% Pe/0.5M HCl solution prior to and following 18CS corrosion test.

results earlier observed, the OCP plots in Fig. 10(a) and (b) shows 18CS at 3.5% Pe concentration in H_2SO_4 and HCl solution exhibited the highest tendency to corrode. Both plots resumed at −0.492 V and −0.428 V (0 s); although the plot in Fig. 10(a) significantly decreased to electronegative values signifying higher vulnerability to corrosion. The plot attained relative thermodynamic stability at 5800.05 s (−0.580 V) before terminating at −0.579 V. This observation differs from the corresponding plot in Fig. 10(b) where it continually progressed to electropositive values after brief electronegative shift to −0.564 V at 400.80 s. The plot terminated at −0.510 V at 10800 s. While the plot at 0% Pe concentration tends to be the most electropositive in Fig. 10(a), the OCP plot at 1% Pe concentration was the most electropositive in Fig. 10(b). This observation shows the interaction of the inhibitor with the metal exterior remains highly reactive despite effective inhibitor protection [55]. This is evident on the thermodynamic instability of the inhibitor protection as evident in the plots

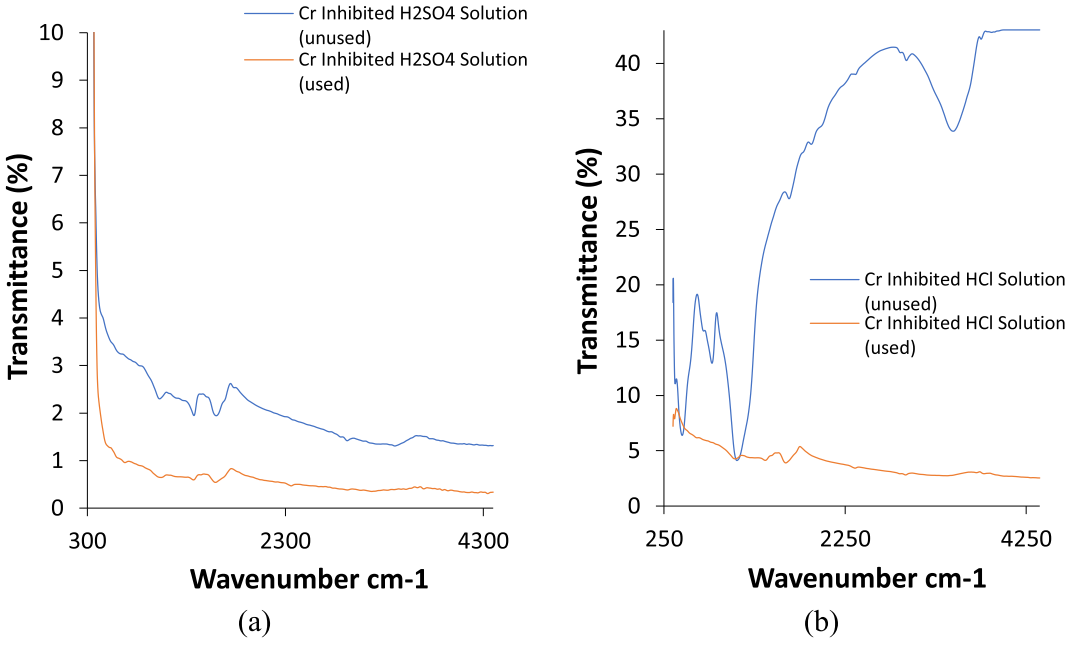

Fig. 14 – ATF-FTIR spectra plots of (a) 1% Cr/0.5M H_2SO_4 solution and (b) 1% Cr/0.5M HCl solution prior to and following 18CS corrosion test.

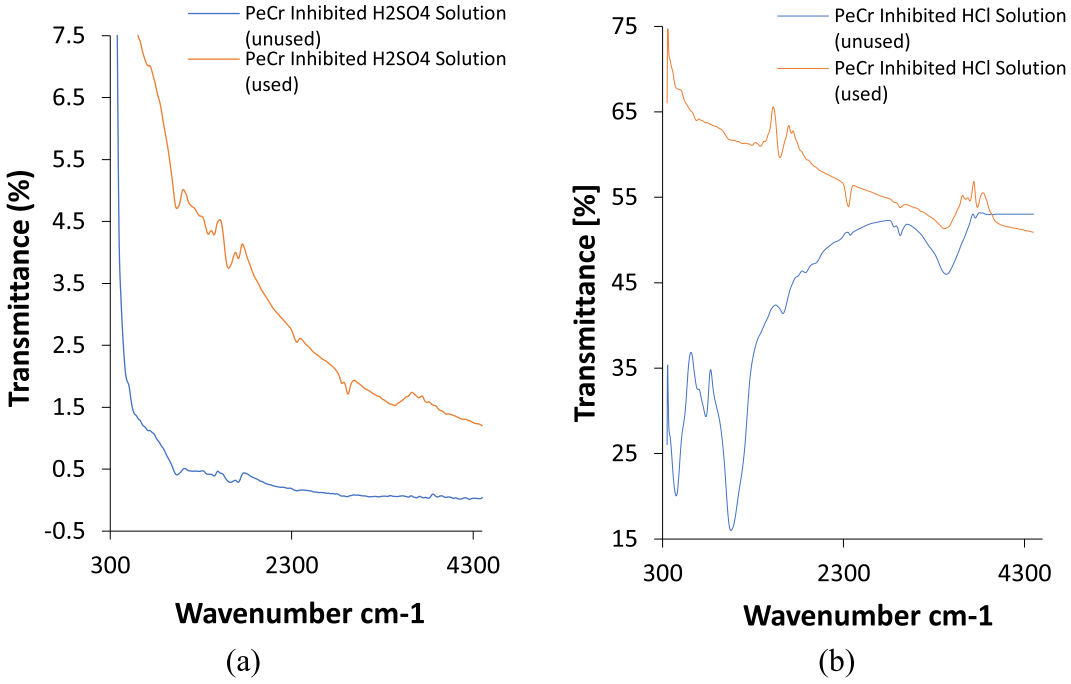

Fig. 15 – ATF-FTIR spectra plots of (a) 1% PeCr/0.5M H_2SO_4 solution and (b) 1% PeCr/0.5M HCl solution prior to and following 18CS corrosion test.

[56]. However, Fig. 10(b) shows the plots at 1% and 3.5% Pe concentration in HCl has a stronger potential to attain electropositive data outputs relative to the plot at 0% Pe concentration.

In Fig. 11(a), Cr concentrate exhibited similar behaviour to Pe concentrate [Fig. 10(a)]. The OCP plot shows Cr at 3.5% concentration exhibited the most electronegative values, initiating at −0.603 V and briefly displaying decrease corrosion tendency till −0.587 V at 611.41 s. Beyond this point, there was increase in tendency to corrode before the plot attained relative stability at 2606.42 s (−0.599 V) till the point of termination. Cr plot at 1% concentration was marginally more electropositive than the plot at 0% Cr concentration. In addition to the reasons earlier mentioned, these observations are also on account of the lateral reaction amidst the inhibitor species in the acid media which strongly influences the electrochemical equilibrium at the metal-electrolyte layer. The plot in Fig. 11(b) conventionally agrees with the polarization and coupon measurement plots where the plot at 0% Cr concentration is most electronegative (higher corrosion tendency) while the plot at 3.5% Cr concentration is most electropositive due to the protective film of Cr over 18CS [57,58]. The film tends to be less passive in HCl compared to H_2SO_4 media. The plot initiated at −0.467 V, transited briefly to higher electropositive values before progressively decreasing to −0.461 V at termination. Similar observation occurred for PeCr in HCl [Fig. 12(b)] where the plot at 0% PeCr concentration is most electronegative while the plot at 1% PeCr was most electropositive and thermodynamically stable compared to the plot at 3.5% PeCr. The OCP plots in Fig. 12(b) exhibited similar observation to Figs. 10(a) and 11(a). It is probable that SO_4^{2-} anions significantly influence the plot configuration in Figs. 10(a) and 11(a) and 12(a) compared to their counterparts in HCl. Generally, SO_4^{2-} anions tends to cause general surface degradation compared to HCl whose corrosive action tends to be localized. Secondly, the ionization potential of SO_4^{2-} anions makes it highly reactive in competition with protonated inhibitor molecules.

3.4. *ATF-FTIR spectroscopy*

Reactive groups within the concentrate molecules and their bonds actively involved in the metal-inhibitor interaction and modification of the corrosive media were determined by ATF-FTIR spectroscopy after correlating with the ATR-FTIR standard Table [59,60]. Tables 7–8 presents the theoretical wavenumber, calculated wavenumber before and after corrosion test, reactive groups and their bond for Pe, Cr and PeCr concentrates in H_2SO_4 and HCl solution. The spectra plot and their peaks prior to and following corrosion test are displayed from Figs. 13–15f. Generally, the calculated wavenumbers of identified reactive groups in H_2SO_4 (Tables 6–8) are carbonyls (general), carboxylic acids, primary amines, ketones, alcohols, aromatics, esters, aliphatic amines, ethers, alkanes, carboxylic acids, alpha and beta–unsaturated aldehydes. In HCl, the corresponding reactive groups identified are carboxylic acids, primary amines, aliphatic amines, alcohols, phenols, alkenes, secondary amines, aromatics, alkyl halides, alkanes, esters

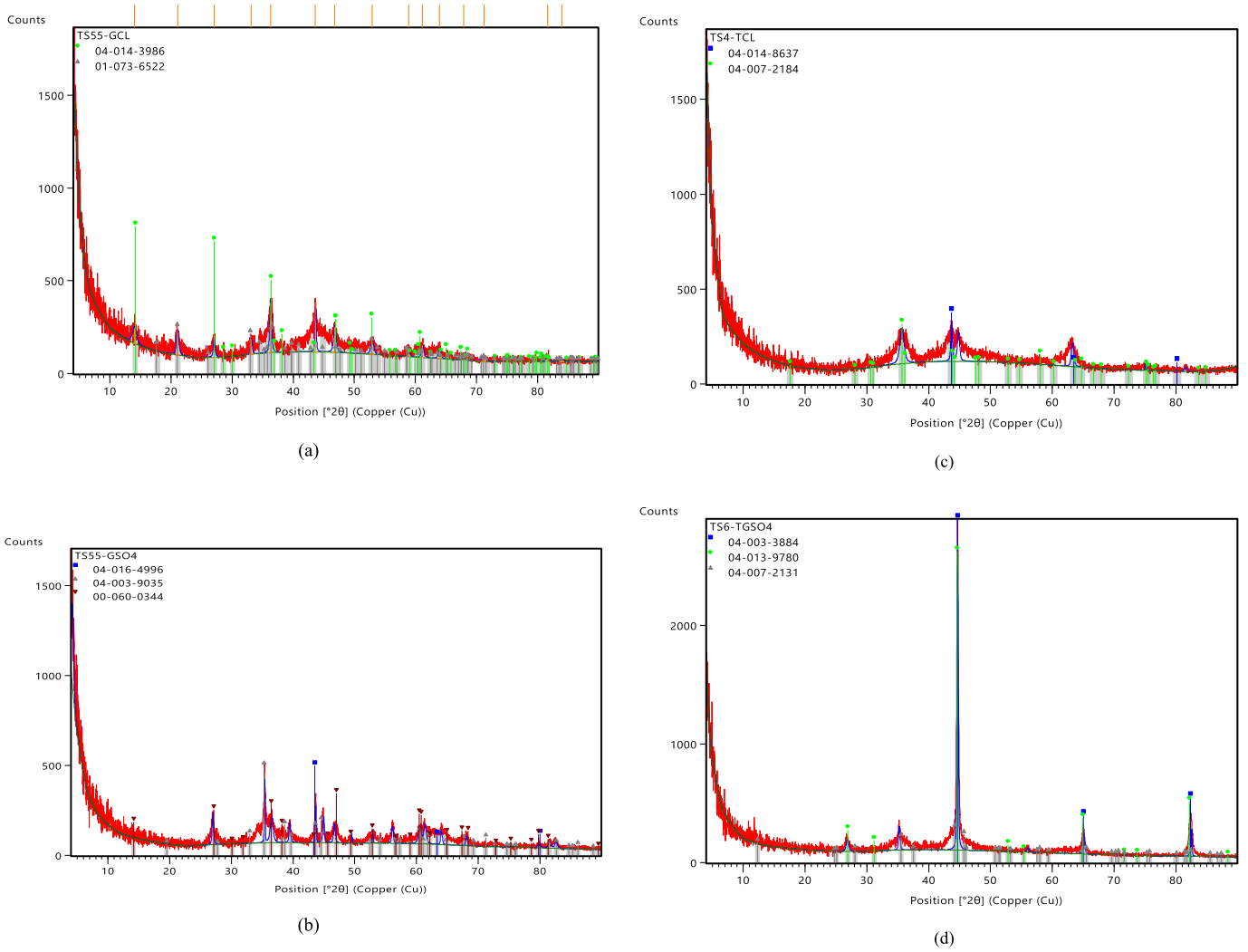

Fig. 16 – Illustrative XRD Phase identification plots for 18CS (a) from H_2SO_4/HCl solution, (b) from H_2SO_4/HCl solution with Pe concentrate, (c) from H_2SO_4/HCl solution with Cr concentrate and (d) from H_2SO_4/HCl solution with PeCr concentrate.

Table 9 – Illustrative identified pattern list for XRD analysis of 18CS in H_2SO_4 and HCl solution in the specific of oil concentrates.

Acid Solution		Gain	Compound Identification	Displ. [°2θ]	Scale Fac.	Chem. Formula
Visible	Ident. Code					
*	04-014-3986	28	Iron Oxide Hydroxide	0	0.339	FeO(OH)
*	01-073-6522	23	Iron Oxide Hydroxide	0	0.47	FeO(OH)
Pe Concentrate						
Visible	Ident. Code	Gain	Compound Identification	Displ.[°2θ]	Scale Fac.	Chem. Formula
*	04-016-4996	41	Iron	0	0.251	Fe
*	04-003-9035	32	Iron Nickel Zirconium	0	0.652	$Zr_2Fe_{0.5}Ni_{0.5}$
Cr Concentrate						
Visible	Ident. Code	Gain	Compound Identification	Displ.[°2θ]	Scale Fac.	Chem. Formula
*	04-014-8637	63	Iron	0	0.489	Fe
*	04-007-2184	52	Copper Oxide	0	0.273	Cu_4O_3
PeCr Concentrate						
Visible	Ident. Code	Gain	Compound Identification	Displ.[°2θ]	Scale Fac.	Chem. Formula
*	04-003-3884	82	Iron	0	0.965	Fe
*	04-013-9780	70	Aluminum Iron	0	0.868	Fe_3Al
*	04-007-2131	17	Copper Phosphide	0	0.064	Cu_3P

and ethers. These reactive groups are the sites through which protonated Pe, Cr and PeCr species in the acid media reacts with the ionized 18CS exterior and suppressing the redox reaction accountable for surface degeneration through evolution of an inert oxide, alteration of the corrosive medium, evolution of non-reactive precipitates on the steel surface etc. [61,62].

The calculated wavenumbers in Tables 6–8 (before and after corrosion) which represents important peaks on the spectra plot tends to decrease or increase and in some cases disappears of appear. This phenomenon is due to the reaction of the concentrates in the acid media in interaction with 18CS surface whereby suppression of the electrochemical reactions on 18CS surface could result in complete absorption of the reactive groups, breakdown of the reactive groups and their respective bonds, increased agglomeration of reactive groups etc. which invariably influences the transmittance values and wavenumbers. The spectra plot in Fig. 13(a) and (b), Fig. 15(a) and (b) shows increased transmittance of reactive groups with respect to wavenumber. This is due to the release/formation of reactive group during corrosion of 18CS wherewith in the case of Figs. 13(a) and 15(a), the reactive groups do not sufficiently influence the electrochemical process to effectively suppress corrosion. Whereas in Fig. 13(b) and (b), the increase transmittance of the reactive groups with respect to wavenumber after corrosion is accountable for the effective corrosion inhibition of the concentrates involved due to formation of surface coverage and strong electrostatic attraction with the steel surface though not likely to be covalent but physiochemical. It must be noted that the spectra plot in Figs. 13(a) and 15(b) do show significant decrease in transmittances indicating strong adsorption at wave numbers 3188 cm^{-1} and 3972 cm^{-1}. i.e. the respective functional groups probably chemically combined with the steel to reduce corrosion. The spectra diagram in Fig. 14(a) and (b) displays substantial decrease in transmittance due to reasons earlier mentioned. The reactive groups strong interactive with 18CS surface i.e. were adsorbed during the corrosion reaction mechanisms. However, the adsorption in Fig. 14(b) translated to effective corrosion inhibition of 18CS in HCl at all Cr concentrations compared to Fig. 14(b).

3.5. *X-ray diffraction analysis*

X-ray diffraction of 18CS following weight loss measurement from H_2SO_4 and HCl electrolytes in the presence and absence of Pe, Ce and PeCr oil concentrates was done. Illustrative diffraction patterns showing the peaks are depicted from Fig. 16(a)–(d). Fig. 16(a) presents the illustrative diffraction peaks for 18CS from the acid electrolytes in the absence of the oil concentrates. Fig. 16(b)–(d) shows the illustrative diffraction peaks of 18CS from the electrolytes with Pe, Ce and PeCr oil concentrates. Table 9 presents the illustrative identified pattern list for 18CS in both acids in the absence and presence of Pe, Ce and PeCr concentrates. The plot in Fig. 16(a) gives peak values at 2Θ = 14.007, 21.076, 27.044, 33.140, 36.284, 43.631, 46.781, 52.909, 58.922, 61.170, 63.906, 67.915, 71.271, 81.613 and 83.993 for 18CS in the absence of the concentrates. The peak values indicate presence of FeO(OH) phase compounds, a corrosion product that appears commonly as rust during corrosion of carbon steels [63,64]. In the presence of Pe concentrate, identified peaks at 2Θ = 4.259, 26.973, 35.354, 36.490, 39.447, 43.639, 44.909, 46.660, 49.507, 52.854, 56.069, 60.524, 61.350, 63.998, 68.072, 79.766, 81.523 and 82.569 indicates Fe and Fe–Ni–Zr phase compounds while the diffraction peaks in the presence of Cr oil concentrate at 2Θ = 35.648, 43.672, 44.788, 63.224, 75.027 and 81.527 indicating Fe and Cu_4O_3 and in the presence of PeCr oil concentrates at 2Θ = 26.846, 35.209, 44.657, 55.995, 65.038 and 82.318 indicates Fe, Fe_3Al and Cu_3P. The identified compounds in the presence of the concentrates are products of electrochemical reactions among the inhibitor species, corrosive anions and the steel surface. However, the do not constitute corrosive precipitates as shown from optical microscopy.

4. Conclusion

Pelargonium and *Citrus reticulata* oil concentrates and their admixture were evaluated for their inhibition effect on 1018 carbon steel in dilute H_2SO_4 and HCl media. *Citrus reticulata* concentrate reacted efficiently in both acid at all concentrations assessed with values signifying stable inhibition mechanism with respect to time and concentration. Performance of *Pelargonium* in HCl was similar to *Citrus reticulata*. However, in H_2SO_4 *Pelargonium* performed poorly at low concentration and effectively at higher concentration. The admixed concentrate performed more effectively than the individual concentrates in HCl but poorly in H_2SO_4 media. The concentrates and their admixture exhibited mixed inhibition properties with dominant cathodic inhibition mechanism. Significant decrease in transmittance of *Citrus reticulata* reactive groups in both acids was observed at all wavenumber due to attachment of the groups onto the steel exterior and accountable for its effective corrosion inhibition. Transmittance of the reactive groups for *Pelargonium* concentrate and the admixed concentrate increased further signifying strong interaction in the acid solution and surface coverage inhibition mechanism through physiochemical reaction. This is more probable for the admixed concentrate were decrease in transmittance of its reactive groups was observed at higher wavenumbers. Open-circuit potential plots show presence of the concentrates in H_2SO_4 solution increases the reactivity of the steel surface and its thermodynamic inclination to corrode despite strong protection effect in some cases. In HCl, significant tendency towards passivation of the steel surface was observed. Optical representations show the concentrates improves the exterior of the steel surface due to effective corrosion inhibition in comparison to the morphology of the unprotected steel surface. X-ray diffractometry plot and identified pattern list reveals the presence of corrosive products on the unprotected steel while the phase compounds identified on the inhibited steel were non-corrosive.

Declaration of Competing Interest

Author declare no conflict of interest.

Acknowledgement

The authors are grateful to Covenant University for making available facilities for this research.

REFERENCES

[1] Erna M, Herdini H, Futra D. Corrosion inhibition mechanism of mild steel by amylose-acetate/carboxymethyl chitosan composites in acidic media. Int J Chem Eng 2019. https://doi.org/10.1155/2019/8514132.

[2] Tait WS. 28 - corrosion prevention and control of chemical processing equipment. 2nd ed. Handbook of Environmental Degradation of Materials; 2012. p. 863–86. https://doi.org/10.1016/B978-1-4377-3455-3.00028-6.

[3] Singh DK, Kumar S, Udayabhanu G, John RP. 4(N, N-dimethylamino) benzaldehyde nicotinic hydrazone as corrosion inhibitor for mild steel in 1M HCl solution: an experimental and theoretical study. J Mol Liq 2016;216:738–46.

[4] Evans R. 2 - selection and testing of metalworking fluids, metalworking fluids (MWFs) for cutting and grinding, fundamentals and recent advances. Amsterdam: Woodhead Publishing Series in Metals and Surface Engineering, Elsevier; 2012. p. 23–78. https://doi.org/10.1533/9780857095305.23.

[5] Adejoro I, Ojo F, Obafemi S. Corrosion inhibition potentials of ampicillin for mild steel in hydrochloric acid solution. J Taibah Univ Sci 2015;9(2):196–202.

[6] Loto RT, Babalola P. Corrosion polarization behavior and microstructural analysis of AA1070 aluminium silicon carbide matrix composites in acid chloride concentrations. Cogent Eng 2017;(1):1422229. https://doi.org/10.1080/23311916.2017.1422229.

[7] Chen R, Li X, Du C, Cheng Y. Effect of cathodic protection on corrosion of pipeline steel under disbonded coating. Corrosion Sci 2009;51:2242–5.

[8] Yabuki A, Tanabe S, Fathona I. Comparative studies of two benzaldehyde thiosemicarbazone derivatives as corrosion inhibitors for mild steel in 1.0 M HCl. Surf Coating Technol 2018;341:71–7.

[9] Craft G. Protecting a pipeline against corrosion: a cost study. 1996. https://www.wateronline.com/doc/protecting-a-pipeline-against-corrosion-a-cos-0001.

[10] Thompson NG, Yunovich M, Dunmire D. Cost of corrosion and corrosion maintenance strategies. Corrosion 2007;25(34).

[11] Bhaskaran R, Bhalla L, Vishal Sarin V. Cost of corrosion protection in Indian oil & petroleum products transmission pipelines - a case study. J Appl Bus Econ Res 2016;14(7):5169–72.

[12] Chigondo M, Chigondo F. Recent natural corrosion inhibitors for mild steel: an overview. J Chem 2016:6208937. https://doi.org/10.1155/2016/6208937.

[13] Solomon MM, Umoren SA. Enhanced corrosion inhibition effect of polypropylene glycol in the presence of iodide ions at mild steel/sulphuric acid interface. J Environ Chem Eng 2015;3(3):1812–26.

[14] de Damborenea J, Conde A, Arenas MA. 3 - corrosion inhibition with rare earth metal compounds in aqueous solutions, rare earth-based corrosion inhibitors. Woodhead Publishing Series in Metals and Surface Engineering; 2014. p. 84–116.

[15] Monticelli C. Corrosion inhibitors, encyclopedia of interfacial chemistry. Surf Sci Electrochem 2018:164–71.

[16] Chen Y, Yang W. Formulation of corrosion inhibitors. IntechOpen; 2019. https://doi.org/10.5772/intechopen.88533.

[17] Ahmed SK, Ali WB, Khadom AA. Synthesis and investigations of heterocyclic compounds as corrosion inhibitors for mild steel in hydrochloric acid. Int J Ind Chem 2019;10:159–73.

[18] Singh A, Talha M, Xu X, Sun Z, Lin Y. Heterocyclic corrosion inhibitors for J55 steel in a sweet corrosive medium. ACS Omega 2017;2(11):8177–86.

[19] Singh A, Ansari KR, Quraishi MA, Kaya S, Banerjee P. The effect of an N-heterocyclic compound on corrosion inhibition of J55 steel in sweet corrosive medium. New J Chem 2019;43(16):6303–13.

[20] Sundaram RG, Sundaravadivelu M. Anticorrosion activity of 8-quinoline sulphonyl chloride on mild steel in 1MHCl solution. J Metall 2016. https://doi.org/10.1155/2016/8095206. 8095206.

[21] Loto RT. Study of the synergistic effect of 2-methoxy-4-formylphenol and sodium molybdenum oxide on the

corrosion inhibition of 3CR12 ferritic steel in dilute sulphuric acid. Results Phys 2017;7:769–76.
[22] Dariva, C.G., Galio, A.F., Corrosion inhibitors – principles, mechanisms and applications. Applications, in Developments in corrosion protection, Aliofkhazraei, M. IntechOpen. http://www.doi.org/10.5772/57255.
[23] Lin B, Tang J, Wang Y, Wang H, Zuo Y. Study on synergistic corrosion inhibition effect between calcium lignosulfonate (CLS) and inorganic inhibitors on Q235 carbon steel in alkaline environment with Cl^-. Molecules MDPI 2020;25:4200. https://doi.org/10.3390/molecules25184200.
[24] Li Y, Zhao P, Liang Q, Hou B. Berberine as a natural source inhibitor for mild steel in 1 M H_2SO_4. Appl Surf Sci 2005;252:1245–53.
[25] Loto CA, Joseph OO, Loto RT. Adsorption and inhibitive properties of Camellia Sinensis for aluminium alloy in HCI. Int J Elect Sci 2014;9(7):3637–49. In press.
[26] Ashassi-Sorkhabi H, Majidi MR, Seyyedi K. Investigation of inhibition effect of some amino acids against steel corrosion in HCl solution. Appl Surf Sci 2004;225:176–85.
[27] ÖZcan M. AC impedance measurements of cysteine adsorption at mild steel/sulphuric acid interface as corrosion inhibitor. J Solid State Electrochem 2008;12:1653–61.
[28] Loto RT, Oghenerukewe E. Inhibition studies of *Rosmarinus officinalis* on the pitting corrosion resistance 439LL ferritic stainless steel in dilute sulphuric acid. Orient J Chem 2016;32(5):2813–32.
[29] Fu J, Li S, Cao L, Wang Y, Yan L, Lu L. L-Tryptophan as green corrosion inhibitor for low carbon steel in hydrochloric acid solution. J Mater Sci 2010;45:979–86.
[30] Bouoidina A, Chaouch M, Abdellaoui A, Lahkimi A, Hammouti B, El-Hajjaji F, et al. Essential oil of "*Foeniculum vulgare*": antioxidant and corrosion inhibitor on mild steel immersed in hydrochloric medium. Anti-Corros Method M 2017;64(5):563–72.
[31] Hamdani I, El Ouariachi E, Mokhtari O, Salhi A, Chahboun N, ElMahi B, et al. Chemical constituents and corrosion inhibition of mild steel by the essential oil of *Thymus algeriensis* in 1.0 M hydrochloric acid solution. Der Pharma Chem 2015;7(8):252–64.
[32] El Ouadi Y, Bouyanzer A, Majidi L, Paolini J, Desjobert JM, Costa J, et al. *Salvia officinalis* essential oil and the extract as green corrosion inhibitor of mild steel in hydrochloric acid. J Chem Pharmaceut Res 2014;6(7):1401–16.
[33] El Ouariachi E, Bouyanzer A, Salghi R, Hammouti B, Desjobert JM, Costa J, et al. Inhibition of corrosion of mild steel in 1 M HCl by the essential oil or solvent extracts of *Ptychotis verticillata*. Res Chem Intermed 2015;41:935–46.
[34] Boumhara K, Tabyaoui M, Jama C, Bentiss F. *Artemisia mesatlantica* essential oil as green inhibitor for carbon steel corrosion in 1 M HCl solution: electrochemical and XPS investigations. J Ind Eng Chem 2015;29:146–55.
[35] Lahhit N, Bouyanzer A, Desjobert JM, Hammouti B, Salghi R, Costa J, et al. Fennel (*Foeniculum vulgare*) essential oil as green corrosion inhibitor of carbon steel in hydrochloric acid solution. Port Electrochim Acta 2011;29(2):127–38.
[36] Pelargonium. Plants of the world online. Kew: Royal Botanic Gardens. https://powo.science.kew.org/taxon/urn:lsid:ipni.org:names:30302759-2.
[37] Kathleen NB. Sunset western garden book. 6th ed. Menlo Park, California: Sunset Pub. Corp; 1995. p. 606–7.
[38] Mitchell EH. Flower pigmentation in pelargonium hortorum. CA grant; 2013. 2704584, 2013.
[39] Pelargoniums - an herb society of America fact sheet. The Herb Society of America; 2006.
[40] Morton JF. Mandarin orange. In: Fruits of warm climates; 1987. p. 142–5.
[41] Yeung H-C. Handbook of Chinese herbal formulas. 2 Ed. Rosemead, CA: Institute of Chinese; 1998 [Medicine].
[42] El Ouadi Y, Bouyanzer A, Majidi L, Paolini J, Desjobert J-M, Costa J, et al. Evaluation of Pelargonium extract and oil as eco-friendly corrosion inhibitor for steel in acidic chloride solutions and pharmacological properties. Res Chem Intermed 2015;39(10):7125–49.
[43] Yamuna J, Antony Noreen. Ecofriendly extract of Citrus reticulata as corrosion inhibitor for copper in NaOH Solution. Int J TechnoChem Res 2015;1(2):102–6.
[44] Chaubey N, Singh VK, Quraishi MA. Effect of some peel extracts on the corrosion behavior of aluminum alloy in alkaline medium. Int J Ind Chem 2015;6:317–28.
[45] Khalid MAA. Introductory chapter: historical and newest perspectives. IntechOpen; 2017. https://doi.org/10.5772/intechopen.68917.
[46] Xihua X, Ambrish S, Zhipeng S, Ansari KR, Lin Yuanhua L. Theoretical, thermodynamic and electrochemical analysis of biotin drug as an impending corrosion inhibitor for mild steel in 15% hydrochloric acid. R Soc Open Sci 2017;4:170933. https://doi.org/10.1098/rsos.170933.
[47] Mathew ZP, Rajan K, Augustine C, Joseph B, John S. Corrosion inhibition of mild steel using poly (2-ethyl -2-oxazoline) in 0.1M HCl solution. Heliyon 2020;6(11):e05560. https://doi.org/10.1016/j.heliyon.2020.e05560.
[48] Fouda AS, El-Desoky HS, Abdel-Galeil MA, Mansour D. Niclosamide and dichlorphenamide: new and effective corrosion inhibitors for carbon steel in 1M HCl solution. SN Appl Sci 2021;3:287.
[49] Saviour AU, Moses MS. Synergistic corrosion inhibition effect of metal cations and mixtures of organic compounds: a Review. J Environ Chem Eng 2017;5(1):246–73.
[50] Shaju KS, Thomas KJ, Raphael VP, Paul A. Synergistic effect of KI on corrosion inhibition of mild steel by polynuclear schiff base in sulphuric acid. Int Sch Res Notices 2012;425878. https://doi.org/10.5402/2012/425878.
[51] Usman BJ, Gasem ZM, Umoren SA, Solomon MM. Eco-friendly 2-thiobarbituric acid as a corrosion inhibitor for API 5L X60 steel in simulated sweet oilfield environment: electrochemical and surface analysis studies. Sci Rep 2019;9(1):830. https://doi.org/10.1038/s41598-018-37049-w.
[52] Al-Baghdadi S, Gaaz TS, Al-Adili A, A Al-Amiery A, Takriff MS. Experimental studies on corrosion inhibition performance of acetylthiophene thiosemicarbazone for mild steel in HCl complemented with DFT investigation. Int J Low-Carbon Technol 2021;16(1):181–8.
[53] Rajendran S, Apparao BV, Palaniswamy N. Corrosion inhibition by phenyl phosphonate and Zn^{2+}. Anti-Corros Meth Mater 1998;45:158–61.
[54] Refaey SAM, Abd El-Rehim SS, Taha F, Saleh MB, Ahmed RA. Inhibition of chloride localized corrosion of mild steel by PO_4^{3-}, CrO_4^{2-}, MoO_4^{2-}, and NO^{2-} anions. Appl Surf Sci 2000;158(3–4):190–6.
[55] Chiter F, Costa D, Maurice V, Marcus P. Corrosion inhibition of locally de-passivated surfaces by DFT study of 2-mercaptobenzothiazole on copper. npj Mater Degrad 2021;5:52. https://doi.org/10.1038/s41529-021-00198-x.
[56] Chakravarthy MP, Mohana KN. Adsorption and corrosion inhibition characteristics of some nicotinamide derivatives on mild steel in hydrochloric acid solution. Int Sch Res Notices 2014:687276. https://doi.org/10.1155/2014/687276.
[57] Alves VA, Christopher MA, Brett CMA. Characterisation of passive films formed on mild steels in bicarbonate solution by EIS. Electrochim Acta 2002;47:2081–91.
[58] Aramaki K, Shimura T. Prevention of passive film breakdown and corrosion of iron in 0.1M KClO4 with and without Cl^- by covering with an ultrathin two-dimensional polymer coating

and healing treatment in 0.1M $NaNO_3$. Corros Sci 2010;52(9):2766–72.
[59] Table of characteristic IR absorptions. http://orgchem.colorado.edu/Spectroscopy/specttutor/irchart.pdf. [Accessed 12 January 2021].
[60] George S. Infrared and Raman characteristic group frequencies: tables and charts. New York: John Wiley & Sons; 2004.
[61] Assad H, Kumar A. Understanding functional group effect on corrosion inhibition efficiency of selected organic compounds. J Mol Liq 2021;117755. https://doi.org/10.1016/j.molliq.2021.117755.
[62] Peme T, Olasunkanmi LO, Bahadur I, Adekunle AS, Kabanda MM, Ebenso EE. Adsorption and corrosion inhibition studies of some selected dyes as corrosion inhibitors for mild steel in acidic medium: gravimetric, electrochemical, quantum chemical studies and synergistic effect with iodide ions. Molecules 2015;20:16004–29.
[63] Oh SJ, Cook D, Townsend H. Characterization of iron oxides commonly formed as corrosion products on steel. Hyperfine Interact 1998;11:59–66. https://doi.org/10.1023/A:1011076308501.
[64] Kim Y-S, Kim J-G, S J. Corrosion behavior of pipeline carbon steel under different iron oxide deposits in the district heating system. Metals 2017;7:182. https://doi.org/10.3390/met7050182.